ChemComm

FEATURE ARTICLE

View Article Online
View Journal | View Issue

Cite this: *Chem. Commun.*, 2025, **61**, 12871

Recent advances in fluorogenic probes based on twisted intramolecular charge transfer (TICT) for live-cell imaging

Hisashi Ohno, [a] Shun Sumitani,[a] Eita Sasaki, [ab] Sota Yamada [ab] and Kenjiro Hanaoka *[ab]

Received 31st March 2025,
Accepted 30th July 2025

DOI: 10.1039/d5cc01802a

rsc.li/chemcomm

Fluorescence imaging is a powerful technique for visualizing biological events in living samples, and new fluorescence-control mechanisms are still needed to extend the scope of biomolecule-targeting fluorogenic probes. Twisted intramolecular charge transfer (TICT) is a unique fluorescence quenching mechanism that depends upon a twisted conformation to promote intramolecular charge separation. Probes utilizing TICT can detect biological molecules/phenomena, such as viscosity, polarity and extended protein structures, that cannot readily be accessed by probes employing other fluorescence-control mechanisms, such as photoinduced electron transfer or spirocyclization. In this review, we summarize recent work on molecular design strategies for TICT-based fluorogenic probes, focusing on structural-modification approaches to control the ease of TICT state formation.

Introduction

Fluorescence imaging is widely used for the analysis of biological phenomena in living cells and tissues, and there is an ongoing need to extend the available range of fluorogenic probes.[1–3] Small-molecule fluorogenic probes have the great advantage that they do not require genetic manipulation, in contrast to fluorescent protein-based probes, and therefore the establishment of versatile fluorescence-control mechanisms, such as photoinduced electron transfer (PeT),[4] is critical for the rational development of new probes. Recently, twisted intramolecular charge transfer (TICT) has attracted increasing attention as a fluorescence-control mechanism. The occurrence of TICT between donor and acceptor moieties results in fluorescence quenching, but if bond rotation is inhibited, TICT state formation is suppressed, resulting in strong fluorescence. Consequently, TICT-based probes can detect biological molecules/phenomena, such as viscosity, polarity and extended protein structures, that are difficult to detect with probes employing other fluorescence-control mechanisms. Although the mechanism of TICT-based fluorescence quenching was reported in the early 2000s,[5] initial efforts to design TICT-based

[a] *Graduate School of Pharmaceutical Sciences, Keio University, Tokyo 105-8512, Japan. E-mail: khanaoka@keio.jp*
[b] *Faculty of Pharmacy, Keio University, Tokyo 105-8512, Japan*

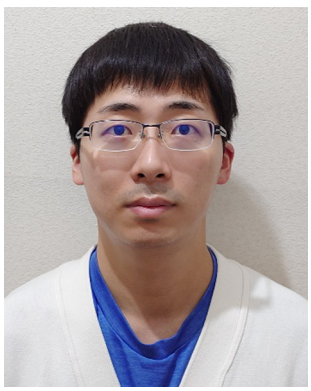

Hisashi Ohno

Hisashi Ohno received his BS in 2016 from the Department of Chemistry, the Faculty of Science, Hokkaido University, and his PhD in 2022 from the Graduate School of Pharmaceutical Sciences, the University of Tokyo. Since 2022, he has worked with Prof. Hanaoka at the Graduate School of Pharmaceutical Sciences, Keio University. His research interests include the development of new small-molecular fluorescence probes for drug discovery.

Shun Sumitani

Shun Sumitani received his BS in 2024 from the Faculty of the Pharmaceutical Sciences, Keio University. Since 2024, he has been a graduate student in the Graduate School of Pharmaceutical Sciences, Keio University. His research interests include the development of fluorescence probes for visualizing biological phenomena.

fluorogenic probes were empirical. However, since the late 2010s, there has been intensive investigation of approaches to control TICT state formation of fluorophores by structural modification. In addition, technical progress in quantum-chemical calculation of the excited states of the fluorophores has promoted the theory-based molecular design of TICT-based fluorogenic probes. In this review, we summarize recent work on TICT-based fluorescence-control methods and we describe molecular design strategies for TICT-based fluorogenic probes having various fluorophores.

1. Mechanism of TICT

TICT is a charge transfer process in which electron donor and acceptor moieties in a molecule are linked by a π-conjugated spacer incorporating rotatable single bonds (Fig. 1a). The TICT state was first clearly recognized when the unique fluorescence properties of 4-(dimethylamino)benzonitrile (DMABN) were reported (Fig. 1b).[6] While many fluorescent molecules emit only from their lowest excited state according to Kasha's rule, the fluorescence spectrum of DMABN has two fluorescence maxima. Subsequent studies revealed that the two fluorescence peaks of DMABN were emitted from the excited singlet state and from the TICT state.[5]

One of the features of dyes that form the TICT state is the structural change in the excited state (Fig. 1a). In general, when a fluorescent molecule absorbs light, it is converted to the emissive state, which is the locally excited (LE) state for non-polar dyes or the intramolecular charge transfer (ICT) state for

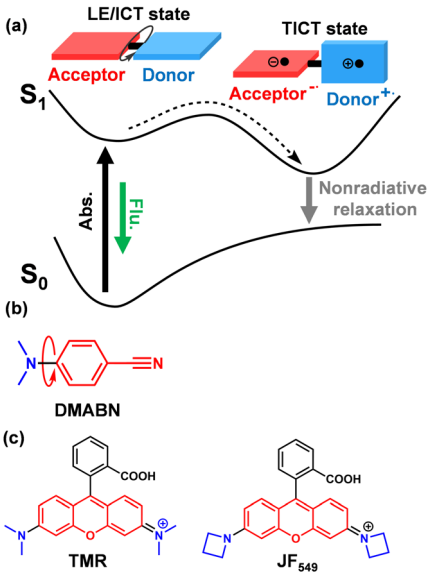

Fig. 1 (a) Schematic illustration of the TICT mechanism. Dyes showing TICT state formation consists of electron donor (blue) and acceptor (red) moieties. Abs.: absorption; Flu.: fluorescence. (b) The structure of DMABN. (c) The structure of TMR and JF_{549}.

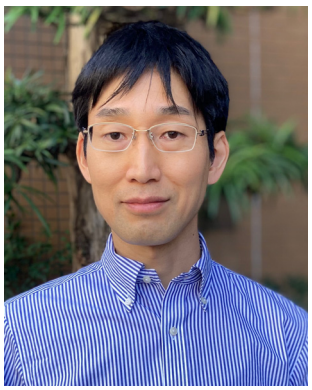

Eita Sasaki

Eita Sasaki received his BS and MS degrees in Pharmaceutical Sciences from the University of Tokyo in 2003 and 2005, respectively. He obtained his PhD in Chemistry from the University of Texas at Austin in 2011. Following postdoctoral research at ETH Zurich, he joined the Graduate School of Agricultural and Life Sciences, the University of Tokyo, as an Assistant Professor in 2017. Since 2021, he has served as a Senior Assistant Professor at the Faculty of Pharmacy, Keio University. His research interests include the development of fluorescence probes and the engineering of self-assembling proteins.

Sota Yamada

Sota Yamada received his BS in 2015 from the Faculty of Pharmaceutical Sciences at Nagoya City University. He studied at the Graduate School of Pharmaceutical Sciences of Kyoto University and became a Project Assistant Professor at the Graduate School of Pharmaceutical Sciences, Keio University in 2019. Since 2021, he has worked with Prof. Hanaoka at the Graduate School of Pharmaceutical Sciences, Keio University. His research interests include the development of nanoprobes for drug delivery system.

Kenjiro Hanaoka

Kenjiro Hanaoka received his BS in 2000 from the Faculty of Pharmaceutical Sciences, the University of Tokyo, and his PhD in 2005 from the Graduate School of Pharmaceutical Sciences, the University of Tokyo. During 2005–2007, he worked with Prof. Kodadek at the University of Texas, Southwestern Medical Center. He became Assistant Professor at the Graduate School of Pharmaceutical Sciences, the University of Tokyo, in 2007, and was promoted to Associate Professor in 2011. He became a Professor at Keio University in 2021. His research interests cover the development of chemical biology tools that can visualize or regulate biological phenomena.

dipolar dyes, and subsequently returns to the ground state with fluorescence emission. On the other hand, dyes forming the TICT state firstly enter the LE/ICT state after photoirradiation, then the ICT nature increases as the dihedral angle between the electron donor and acceptor moieties increases (see Fig. 1a). When the dihedral angle is around 90 degrees, a TICT state is formed in which one electron is transferred from the donor to the acceptor. In many dye molecules, the TICT state is converted to the ground state through non-radiative relaxation, showing no fluorescence.

2. Highly fluorescent dyes utilizing inhibition of TICT state formation

Based on the above understanding of the fluorescence quenching mechanism associated with TICT state formation, various attempts have been made to develop highly fluorescent dyes. For example, the introduction of an intramolecular chemical crosslink into the dye structure is a classical modification method to suppress TICT state formation,[7–9] *i.e.*, the intramolecular crosslink blocks the rotation between the electron donor and acceptor moieties. Lavis's group reported that the introduction of azetidinyl groups increases the fluorescence quantum yield of rhodamines (Fig. 1c).[10] They found that the fluorescence quantum yield of JF_{549}, in which the dimethylamino groups of tetramethylrhodamine (TMR) were replaced by azetidinyl groups, was markedly increased from 0.41 to 0.88 in aqueous solutions with little effect on other photophysical properties, or on biocompatibility. Further, they demonstrated that this azetidinyl-based design strategy was also applicable to other fluorophores, including C-rhodamine, Si-rhodamine, rhodol, coumarin, naphthalimide, oxazine and acridine derivatives. They attributed the enhanced brightness of the azetidine-substituted fluorophores to the inhibition of TICT state formation, on the basis that the azetidine moiety is less sterically repulsive to the fluorophore backbone. Further, cyclic amines with strongly electron-withdrawing groups, such as quaternary piperazine and thiomorpholine 1,1-dioxide, were introduced into various fluorophore scaffolds, resulting in more intense fluorescence.[11,12] This is due to the decreased electron-donating ability of the amino groups on the fluorophore backbone, leading to suppression of TICT state formation. Further, it was reported that β-carbonyl substituents on the electron donor moiety can also inhibit TICT state formation by reducing the interaction of the solvent with the donor structure.[13,14]

3. TICT-based design strategies for fluorogenic probes

Many fluorogenic probes utilizing TICT-based fluorescence quenching have been reported. Recently, chemical derivatizations to control TICT state formation have been extensively investigated, and several molecular design strategies for TICT-based fluorogenic probes targeting different features of the TICT state have been established. Here, we describe some examples.

3.1. Intramolecular rotation

Twisting between the electron donor and acceptor moieties is critical for TICT state formation. If the rotation between the donor and acceptor moieties is inhibited by environmental factors, such as protein binding or viscosity increase, TICT state formation is suppressed, resulting in strong fluorescence.

The TICT mechanism had been empirically utilized as a fluorescence control principle in several fluorogenic probes before the mechanistic details were elucidated. A representative fluorogenic probe based on the TICT mechanism is thioflavin T (Fig. 2).[15] Thioflavin T is composed of an electron acceptor moiety, benzothiazole, and an electron donor moiety, dimethylaniline, and its fluorescence is weak due to strong quenching through the TICT mechanism (Fig. 2a). However, when thioflavin T binds to amyloid beta (Aβ) peptide oligomers, it shows strong fluorescence due to the inhibition of rotation between the electron acceptor and donor moieties (Fig. 2b).[16–18]

SYBR green I, one of the gold-standard DNA-staining reagents, intercalates with DNA (Fig. 3a). This inhibits intramolecular rotation between the electron donor and acceptor moieties of SYBR green I, causing it to become strongly fluorescent.[19] Moreover, the introduction of substituents around the electron donor or acceptor structure increases the steric hindrance, which favors TICT state formation. When this intramolecular steric hindrance is removed upon reaction with the target molecule, the fluorescence intensity of the fluorophore increases. For example, our group reported a fluorogenic probe for the drug-metabolizing enzyme CYP3A4, 2-Me PeER. The fluorescence of 2-Me PeER is quenched through TICT state formation promoted by intramolecular steric hindrance involving the methyl group at the 2-position of the xanthene ring (Fig. 3b).[20] When the alkyl chain on the amino group on the xanthene ring is cleaved by CYP3A4, the steric hindrance is eliminated and the probe becomes highly fluorescent.

3.2. Sensitivity to environmental polarity

In general, compared to the LE/ICT state, the TICT state has a larger intramolecular charge separation between the electron donor and acceptor moieties. The TICT state tends to be stabilized in highly polar environments due to strong solvation,

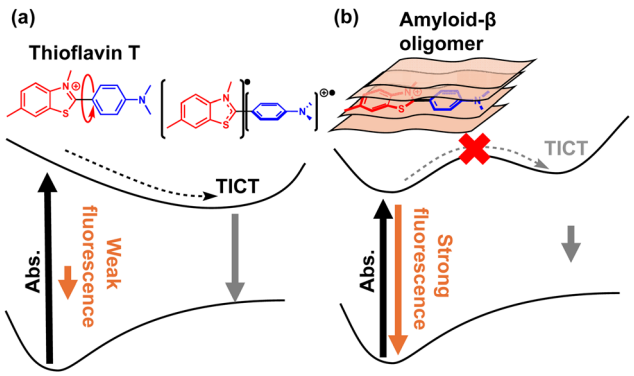

Fig. 2 Schematic illustration of the TICT mechanism of thioflavin T in (a) aqueous solution and (b) bound to Aβ oligomers. Abs.: absorption.

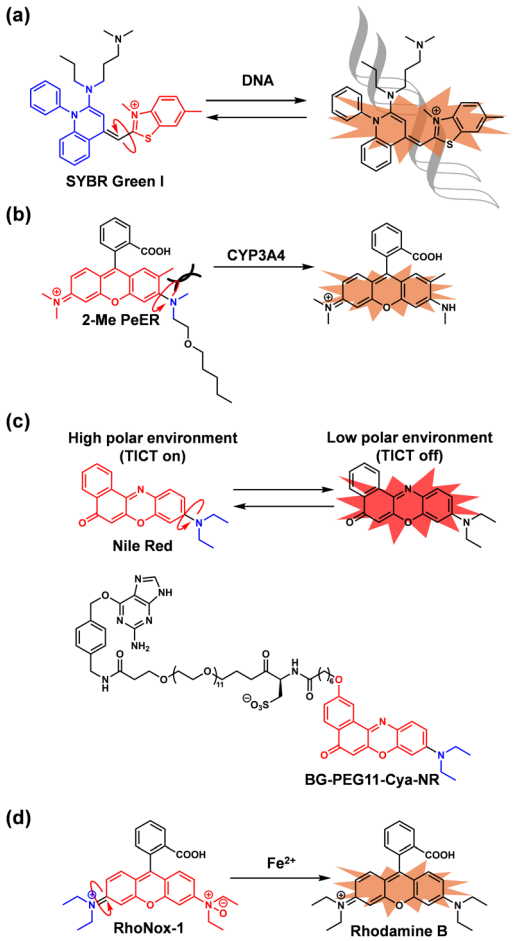

Fig. 3 Examples of TICT-based fluorogenic probes: (a) the DNA-staining reagent, SYBR green I. (b) The fluorogenic probe for CYP3A4, 2-Me PeER. (c) The fluorogenic probe for detecting lipid-rich environments, Nile red, and the Nile red-based probe for SNAP-tagged plasma membrane proteins. (d) The fluorogenic probe for Fe^{2+}, RhoNox-1.

whereas it is destabilized in low-polarity environments due to a lack of solvation. Many fluorogenic probes, including Nile red (Fig. 3c), that can detect low-polarity environments have been developed by utilizing this characteristic environmental polarity-dependent fluorescence change.[21] Fluorescence probes for lipid membranes have also recently been developed, consisting of environment (polarity and viscosity)-sensitive fluorophores, such as aminocoumarins, cyanines, BODIPYs, Nile red derivatives and so on, linked to plasma membrane anchors.[22] For example, Prifti *et al.* described a fluorogenic probe for SNAP-tagged plasma membrane proteins, BG-PEG11-Cya-NR, based on Nile red (Fig. 3c).[23]

3.3. Charge transfer between electron donor and acceptor moieties

Intramolecular charge separation between the electron donor and acceptor moieties occurs during TICT state formation. The driving force for this charge separation depends on the electron-donating and -accepting abilities of the two structures. Consequently, fluorogenic probes emit strong fluorescence when the electron donor or acceptor ability is reduced upon reaction with the target molecule. RhoNox-1, a fluorogenic probe for Fe^{2+}, is fluorescently quenched through the TICT mechanism, *i.e.*, the electron-accepting ability of the xanthene ring is increased by the *N*-oxide group (Fig. 3d).[24] On the other hand, when the *N*-oxide group is reduced by Fe^{2+}, the electron-accepting ability of the xanthene ring decreases, suppressing TICT state formation of the dye.

4. Fluorophores for TICT-based fluorogenic probes

TICT-based fluorogenic probes utilizing various fluorophores such as cyanine, coumarin, 1,8-naphthalimide, BODIPY, rhodamine and others have been reported. In this section, examples of TICT-based fluorogenic probes are described, focusing on the fluorophores.

4.1. Cyanine dyes

Many cyanine dyes show red to near-infrared (NIR) fluorescence with a high absorption coefficient ($>10^5$ M^{-1} cm^{-1}), high brightness and good biocompatibility. Consequently, they have been used as scaffolds for many fluorescent reagents.[25] They are typically donor–π–acceptor type molecules consisting of two nitrogen or oxygen centers and a polymethine chain (Fig. 4). Symmetric cyanines contain electron-donating and -accepting moieties with the same structure, which function interchangeably. On the other hand, asymmetric cyanines contain electron-donating and -accepting moieties with different structures, and their functions are generally not interchangeable. Cyanines readily form the TICT state because the polymethine chain can freely rotate,[5] so most of the empirically developed TICT-based fluorogenic probes are based on the cyanine scaffold (Fig. 4).

A representative TICT-based fluorogenic probe based on cyanine dye can be used to visualize intracellular viscosity. As already noted, formation of the TICT state is suppressed in a highly viscous environment, so the intracellular viscosity can be monitored in terms of fluorescence change. Indeed, fluorogenic probes that target particular intracellular locations have been developed and used to visualize the viscosity in mitochondria (YPE)[26] and lysosomes (IG-Lyso)[27] inside cells (Fig. 4a). *meso*-Substituted cyanine dyes with different sensitivity to rotation-restricted environments (viscosity) have also been used for cellular imaging.[28,29]

TICT-based fluorescence modulation has also been employed to develop DNA-staining agents (Fig. 4b). Ethidium bromide, a conventional DNA-staining reagent, is highly carcinogenic, and therefore alternatives such as thiazole orange and the SYBR series (SYBR green I, PicoGreen, SYBR Safe and SYBR Gold) have been developed.[19,30,31] In the SYBR series, the acceptor structure typically includes a benzothiazole or benzoxazole ring. These dyes exhibit strong fluorescence quenching *via* the TICT mechanism due to free donor–acceptor bond rotation. Upon intercalation with DNA, for which the dyes

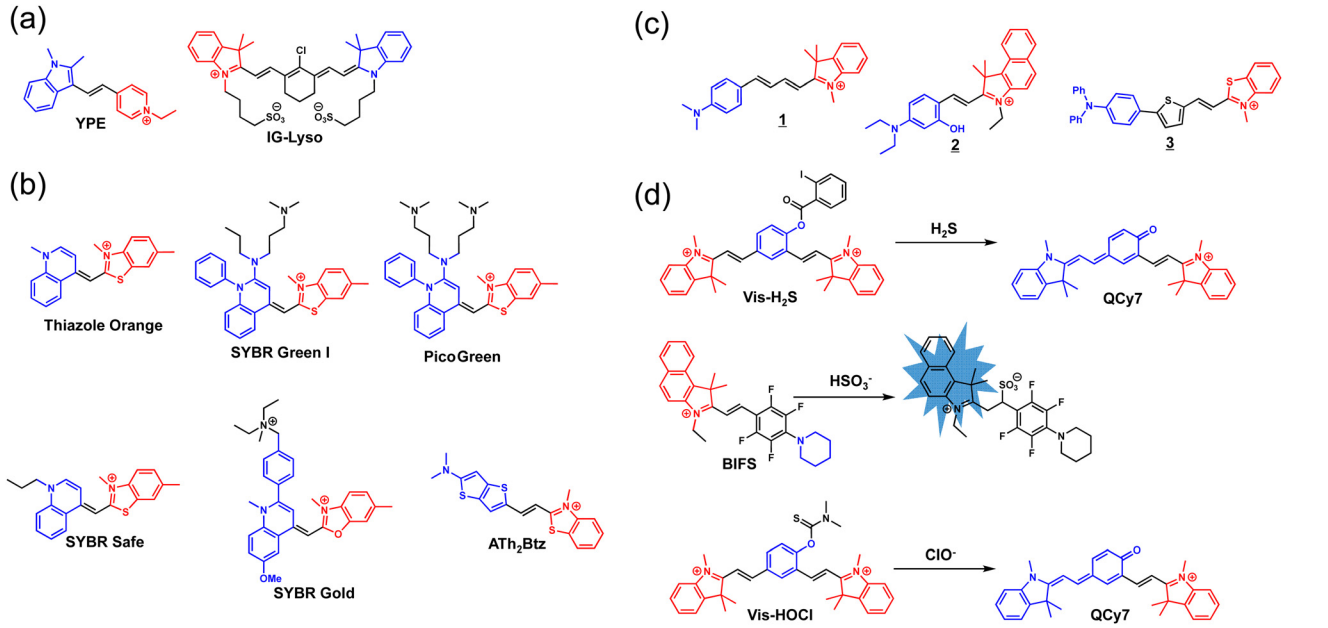

Fig. 4 TICT-based fluorogenic probes having the cyanine scaffold. Fluorogenic probes for (a) viscosity, (b) DNA, (c) HSA/BSA, (d) RSS/ROS. The blue and red structures are the electron-donating and -accepting moieties, respectively.

exhibit high affinity, the bond rotation is restricted, resulting in strong fluorescence emission. A far-red-fluorescent molecular rotor, ATh2Btz, ($\lambda_{ex}/\lambda_{em}$ = 655/677 nm) that can visualize DNA has also been developed (Fig. 4b).[32]

Fluorogenic probes have been developed for the quantitative detection of albumin, the most abundant protein in blood plasma. The main mechanism of the fluorescence emission is inhibition of intramolecular rotation and/or the change in polarity upon binding to the protein surface. Interestingly, small differences in the molecular structures of these probes can result in selectivity of the fluorescence increase for bovine serum albumin (BSA) or human serum albumin (HSA), presumably because of the structural difference of the binding site between BSA and HSA. Reja *et al.* designed a NIR-fluorescence probe **1** for detection of HSA (Fig. 4c).[33] Their probe contains a donor–π–acceptor system and its fluorescence is suppressed due to TICT state formation. In the presence of HSA, **1** binds to a hydrophobic pocket, resulting in the restriction of its molecular rotation. Consequently, the NIR fluorescence of the probe is increased (680 nm). A TICT-based fluorogenic probe **2** for detecting serum albumin was also reported (Fig. 4c).[34] This probe contains a donor–π–acceptor system in which fluorescence is quenched through the TICT mechanism. The probe **2** self-assembles to form molecular aggregates in the absence of albumin, while binding of the probe to albumin triggers disassembly of the aggregates. This specific interaction between **2** and albumin results in fluorescence enhancement due to the suppression of TICT state formation. The same group developed a dual-color fluorogenic probe **3** based on the TICT mechanism (Fig. 4c).[35] The probe **3** exhibits green fluorescence in low-polarity solvents such as toluene, but fluoresces in the far-red/NIR region in high-polarity solvents such as water. Further, IG-Lyso (Fig. 4a) and its analogues covalently bound with the protein can serve as bright near-infrared-II (over 1000 nm) fluorophores for *in vivo* fluorescence imaging of whole animals.[36–38] TICT-based fluorogenic probes targeting reactive sulfur and oxygen species (RSS and ROS) have also been synthesized. Hu *et al.* developed Vis-H_2S as a fluorogenic probe that can visualize both viscosity and H_2S (Fig. 4d).[39] Vis-H_2S is fluorescently quenched through the TICT mechanism, but emits green fluorescence at 492 nm as the environmental viscosity is increased. The probe also has a 2-iodobenzoate ester structure that is converted to weakly fluorescent QCy7 upon reaction with H_2S, altering the electron-donating ability of the donor moiety. The fluorescence of QCy7 is also partially quenched through the TICT mechanism and its fluorescence intensity at 687 nm increases with increasing environmental viscosity. Further, BIFS has been developed as a colorimetric and ratiometric fluorescence probe for HSO_3^- (Fig. 4d).[40] This probe is based on the nucleophilic attack of HSO_3^- on the polymethine chain of the fluorophore. The nucleophilic addition of HSO_3^- to the probe interferes with TICT state formation and this leads to a fluorescence decrease at 592 nm, while the fluorescence at 465 nm increases. There is a good linear relationship between the ratio of the fluorescence intensity (FI_{465}/FI_{592}) and the concentration of HSO_3^-. Vis-HOCl has been reported as a fluorescence probe for HOCl (Fig. 4d).[41] This probe combines the PeT and TICT mechanisms. Its *N*,*N*-dimethylaminothiocarbamate structure selectively reacts with HOCl and acts as an electron acceptor in the PeT process. Vis-HOCl does not show a fluorescence increase even in highly viscous environments due to fluorescence quenching *via* the PeT process. However, when Vis-HOCl reacts with HOCl, it is converted to QCy7, which shows a viscosity-dependent fluorescence increase at 700 nm due to

inhibition of fluorescence quenching through the TICT mechanism in high viscosity environments.

4.2. 7-Aminocoumarin

7-Aminocoumarin has been utilized as a fluorophore of many fluorogenic probes because of its excellent fluorescence properties and ease of synthesis.[42] 7-Aminocoumarin has two stable excited states: an ICT state in which it emits fluorescence in the excited state and a TICT state in which it hardly emits fluorescence (Fig. 5).[5] In these states, the coumarin skeleton acts as an electron acceptor and the amino group serves as an electron donor. In polar solvents, the charge-separated TICT state is stabilized by strong solvation and the compound becomes weakly fluorescent, while in non-polar solvents, the ICT state, which involves less charge-separation than the TICT state due to its planar, non-twisted conformation, is more stable and becomes highly fluorescent.[43,44] Application of the fluorescence enhancement of 7-aminocoumarin by destabilization of its TICT excited state in hydrophobic environments has been investigated for a long time: In the 1990s, it was reported that diethylaminocoumarin shows increased fluorescence upon binding to the hydrophobic pocket of BSA.[45]

Several 7-aminocoumarin-based fluorogenic probes that can detect intracellular viscosity have been reported. Their fluorescence or fluorescence lifetime change is mainly due to the inhibition of intramolecular rotation following the suppression of the TICT state formation in high-viscosity environments. Chen *et al.* synthesized a fluorogenic probe, ACI, containing diethylaminocoumarin as an electron donor and 1,3-indandione as an electron acceptor, that can visualize intracellular viscosity (Fig. 6a).[46] Due to TICT state formation, ACI shows very weak fluorescence. However, the probe exhibits a viscosity-dependent fluorescence increase. A fluorogenic probe, Mito-VCI, that can visualize mitochondrial viscosity, was also reported (Fig. 6a).[47] This probe shows elongation of the fluorescence lifetime with increasing viscosity due to the inhibition of TICT state formation. Mito-VCI has a benzo[e]indolium moiety as an electron acceptor and the coumarin structure serves as an electron donor for TICT state formation. Mito-VCI localizes to mitochondria in cells and could visualize changes of mitochondrial viscosity. Another fluorogenic probe, WSP-1, that can visualize viscosity contains an electron acceptor conjugated to diethylaminocoumarin, and its fluorescence is strongly quenched through the TICT mechanism in aqueous solutions (Fig. 6a).[48] This probe exhibits a viscosity-dependent increase in fluorescence and photoacoustic signals, and was employed for *in vivo* NIR fluorescence and photoacoustic imaging.

Fluorogenic probes based on the change in electron-accepting ability of the coumarin skeleton have been reported. For example, CMBT, can detect mitochondrial sulfur dioxide (SO_2) and viscosity (Fig. 6b).[49] CMBT consists of a diethylaminocoumarin moiety and a benzothiazolium moiety connected *via* a polymethine linker, and is fluorescently quenched through the TICT mechanism in aqueous solution. The probe shows a fluorescence increase at 690 nm or 500 nm due to the inhibition of TICT state formation upon inhibition of intramolecular rotation in response to increased viscosity or upon nucleophilic attack of HSO_3^-/SO_3^{2-} on the polymethine chain moiety. CMBT localizes to mitochondria and could detect viscosity change and endogenous SO_2 in live-cell fluorescence imaging. A fluorogenic probe, XBL, which can detect $ONOO^-$, was also reported (Fig. 6b).[50] XBL contains a diethylaminocoumarin

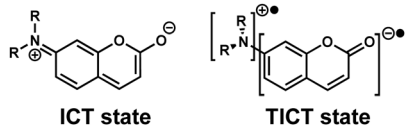

Fig. 5 Structures of 7-aminocoumarins in the ICT and TICT states.

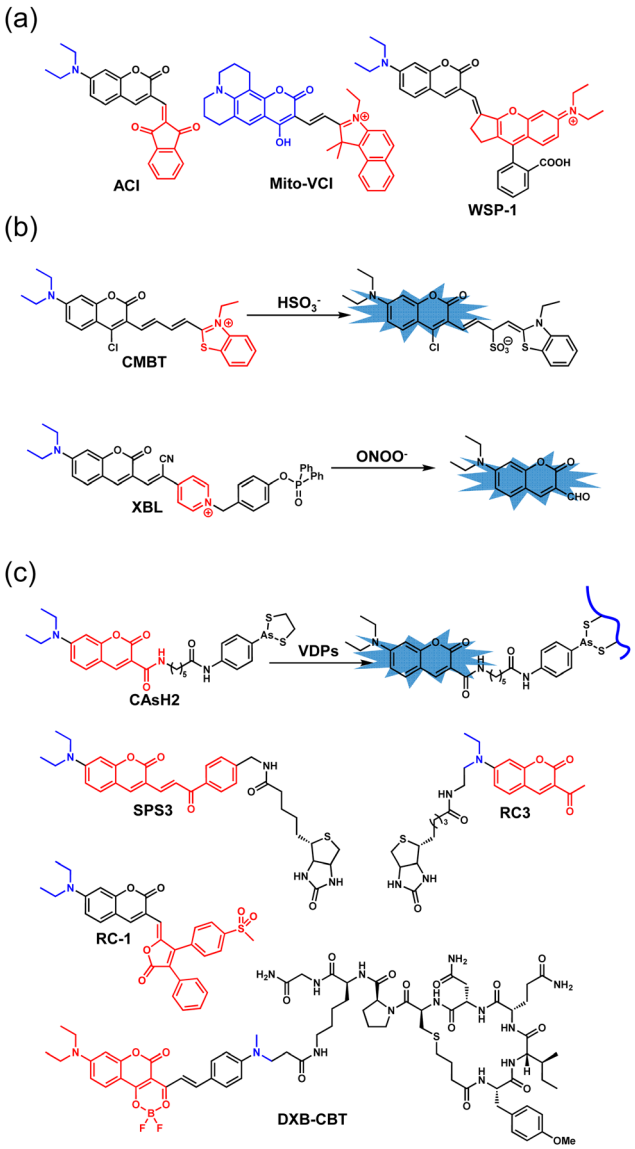

Fig. 6 TICT-based fluorogenic probes having the aminocoumarin scaffold. Fluorogenic probes for (a) viscosity, (b) RSS and ROS, (c) peptides and proteins. The blue and red structures are the electron-donating and -accepting moieties, respectively.

fluorophore and a pyridinium cation moiety as an electron acceptor, and its fluorescence is strongly quenched through the TICT mechanism. XBL reacts with $ONOO^-$ and the pyridinium cation moiety is released, resulting in blue fluorescence emission. XBL localizes to mitochondria and could visualize endogenous $ONOO^-$ in live-cell fluorescence imaging.

Recently, several coumarin-based probes for peptides and proteins have been developed. One such fluorogenic probe, CAsH2, targets vicinal dithiol-containing proteins (VDPs) (Fig. 6c).[51] Aminocoumarins are reported to emit from both the excited ICT and TICT states in polar environments, but only from the ICT state in low-polarity environments, where the TICT state becomes unstable.[52,53] In aqueous solutions, CAsH2 shows weak fluorescence (550 nm) from the TICT excited state, but when bound to VDPs, it shows strong fluorescence (468 nm) from the ICT excited state. Two fluorogenic probes, SPS3 and RC3, which can selectively detect streptavidin and avidin, were also reported (Fig. 6c).[54] SPS3 and RC3, like other aminocoumarins, show weak fluorescence due to the stabilization of their TICT excited state in water. These probes exhibit a large fluorescence increase when bound to streptavidin or avidin. SPS3 is highly selective for streptavidin and RC3 is highly selective for avidin. SPS3 could detect streptavidin expression in live-cell fluorescence imaging. Anwar *et al.* developed RC-1 as an NIR fluorogenic probe that can visualize mitochondrial viscosity and Aβ (Fig. 6c).[55] RC-1 has a diethylaminocoumarin fluorophore and half-tetraphenylethane with an electron-withdrawing group as an electron acceptor, and its fluorescence is strongly quenched *via* a TICT process. In live-cell fluorescence imaging, RC-1 was localized to mitochondria and could visualize the viscosity change there. RC-1 also shows a fluorescence increase upon binding to Aβ and could image Aβ plaques in mouse brain *in vivo*. Moreover, Karpenko *et al.* reported a fluorogenic probe, DXB-CBT, that can detect oxytocin G protein-coupled receptor (Fig. 6c).[56] In the dioxaborine structure of DXB-CBT, the enol and ketone oxygen atoms are cross-linked by a boron atom and this moiety functions as an electron acceptor. DXB-CBT is composed of the dioxaborine moiety, the aniline moiety as an electron donor and the carbetocin moiety as a ligand for oxytocin G protein-coupled receptor. DXB-CBT showed weak fluorescence in water, but emitted 1200 times stronger fluorescence in 1,4-dioxane than in water, because it forms a TICT state involving the dioxaborine and aniline moieties in water, but not in 1,4-dioxane. In live-cell fluorescence imaging, DXB-CBT could visualize oxytocin G protein-coupled receptors expressed on the surface of the cell membrane.

4.3. 1,8-Naphthalimide

1,8-Naphthalimide has a high fluorescence quantum yield and is easily derivatized. Consequently, many fluorogenic probes based on a 1,8-naphthalimide scaffold have been reported.[57] One of the characteristics of 1,8-naphthalimide is that its role in TICT state formation changes depending upon the substituent at the 4-position of the 1,8-naphthalimide scaffold (Fig. 7). When the 4-position is connected to an alkylated amino group or an alkylated amino group *via* a linker having a π-conjugated system, the 1,8-naphthalimide moiety acts as an electron acceptor and the alkylated amino group acts as an electron donor to enable TICT state formation. On the other hand, when a hydroxyl group is introduced at the 4-position, the 1,8-naphthalimide moiety functions as an electron donor, and the TICT state can be formed through conjugation of an electron acceptor moiety to the probe, leading to fluorescence quenching. By selecting a suitable electron donor or acceptor moiety, 1,8-naphthalimide-based probes have been developed to target the local intracellular environment, ROS, endogenous proteins, metal ions, *etc.*

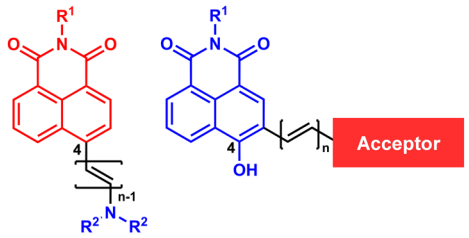

Fig. 7 Molecular design of TICT-based fluorogenic probes having the 1,8-naphthalimide scaffold. The blue and red structures are electron-donating and -accepting moieties, respectively.

Several probes that can detect intracellular viscosity have been reported. The changes in fluorescence intensity or lifetime with increasing viscosity are mainly due to the inhibition of their intramolecular rotation leading to the suppression of TICT state formation. Notably, different molecular structures exhibit different subcellular localizations. Ratiometric probes that can quantify the viscosity in various organelles have been developed. Wei *et al.* described a fluorogenic probe, **4**, that can visualize mitochondrial viscosity (Fig. 8a).[58] Compound **4** has a benzoxazole moiety as the electron acceptor and a hydroxynaphthalimide moiety as the electron donor. The fluorescence intensity of **4** increases in a viscosity-dependent manner. In live-cell fluorescence imaging, **4** could detect changes of mitochondrial viscosity in the cells. Another fluorogenic probe, **5**, which can detect intracellular viscosity, was also reported (Fig. 8a).[59] Compound **5** is composed of 1,8-naphthalimide and anthracene moieties, and shows both a fluorescence increase and a fluorescence lifetime elongation with increasing solvent viscosity. The ratio of the emission intensities at 540 nm and 415 nm and the fluorescence lifetime at 540 nm of **5** are linearly correlated with the solvent viscosity on a logarithmic scale, and were used to quantify viscosity. They also demonstrated that fluorescence ratiometric and lifetime imaging with **5** can quantitatively map intracellular viscosity. Further, a fluorogenic probe, WD-1, which contains a 1,3-indanedione electron acceptor and a hydroxynaphthalimide electron donor (Fig. 8a),[60] could visualize the change in the viscosity of lipid droplets (LDs) in cells and zebrafish.

Probes capable of detecting local polarity in cells have also been reported. Their fluorescence change is based on a change in the stability of the TICT state in response to changes in environmental polarity. Since an organelle-targeting structure

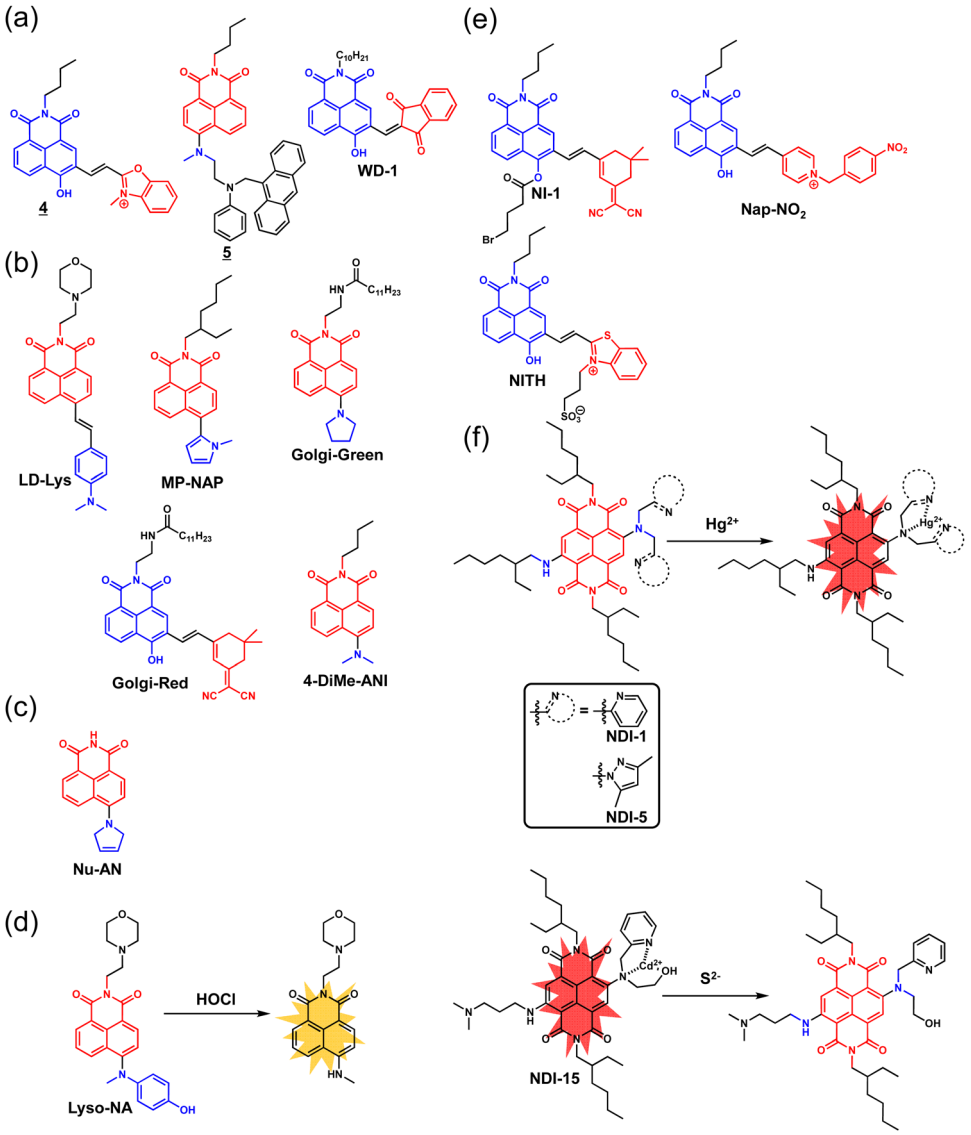

Fig. 8 TICT-based fluorogenic probes having the 1,8-naphthalimide scaffold. Fluorogenic probes for (a) viscosity, (b) polarity, (c) RNA, (d) hypochlorous acid, (e) HSA/BSA and (f) metal ions. The blue and red structures are electron-donating and -accepting moieties, respectively.

can be introduced into these probes, they can detect the polarity change in specific organelles. Meng *et al.* reported a fluorogenic probe, LD-Lys, that can visualize LDs and lysosomes simultaneously (Fig. 8b).[61] The probe localized to LDs and lysosomes in cells, and showed strong fluorescence at 580 nm in LDs and weak fluorescence at 600 nm in lysosomes. Miao *et al.* disclosed a fluorogenic probe, MP-NAP, for LDs (Fig. 8b).[62] The introduction of an *N*-methylpyrrole group into the 1,8-naphthalimide scaffold induced a pre-twisted structure of the probe due to the steric hindrance of the methyl group, and this enhanced the fluorescence quenching by TICT state formation. MP-NAP showed weak fluorescence in aqueous solutions, while it showed strong fluorescence in dichloromethane. In live-cell fluorescence imaging, MP-NAP could stain LDs in the cells without the need to wash out excess probe. Feng *et al.* presented fluorogenic probes, Golgi-Green and Golgi-Red, that can visualize the polarity of the Golgi apparatus (Fig. 8b).[63] In Golgi-Green, the 1,8-naphthalimide moiety acts as an electron acceptor and the tetrahydropyrrole moiety as an electron donor. In Golgi-Red, the malononitrile moiety acts as an electron acceptor and the 4-hydroxy-1,8-naphthalimide moiety acts as an electron donor. Golgi-Green and Golgi-Red show opposite fluorescence responses to polarity change. Golgi-Green showed a fluorescence increase at 530 nm with decreasing polarity, while Golgi-Red unexpectedly showed a fluorescence increase at 720 nm with increasing polarity. In live-cell fluorescence imaging, Golgi-Red could detect the polarity increase in the Golgi apparatus of cells. Michel *et al.* developed a fluorogenic probe, 4-DiMe-ANI, for the wash-free fluorescence imaging of LDs (Fig. 8b).[64] This probe exhibits a high fluorescence quantum yield ($\Phi_{fl} > 0.90$) in non-polar solvents (toluene, $CHCl_3$ and CH_2Cl_2) and shows almost no fluorescence in protic

and polar solvents (ethanol, methanol and PBS). In live-cell fluorescence imaging, 4-DiMe-ANI showed high photofading resistance and high selectivity for LDs in cells.

Jiang *et al.* reported Nu-AN as a fluorogenic probe that can selectively visualize nucleolar RNA (Fig. 8c).[65] The fluorescence of Nu-AN was quenched through the TICT process in aqueous solutions, but upon binding to RNA, its fluorescence at 530 nm increased. In fluorescence recovery (FRAP) experiments, Nu-AN bound to RNA was photodegraded but the fluorescence signal from the RNA was still maintained, probably because Nu-AN can bind RNA reversibly, so that a fresh Nu-AN molecule can replace degraded Nu-AN on the RNA. Further, Nu-AN could label nucleoli in living cells, enabling detailed visualization of their morphology.

Wu *et al.* described a fluorogenic probe, Lyso-NA, that can detect hypochlorous acid in lysosomes (Fig. 8d).[66] Lyso-NA is composed of an aminophenol electron donor, a 1,8-naphthalimide electron acceptor and a morpholine group for lysosome-targeting. The aminophenol and 1,8-naphthalimide moieties form a TICT state, resulting in weak fluorescence of the probe, and Lyso-NA exhibited a hypochlorous acid-selective fluorescence increase. Lyso-NA could detect the production of endogenous hypochlorous acid in zebrafish *in vivo*.

1,8-Naphthalimide-based probes capable of detecting BSA/HSA have also been reported. Ke *et al.* synthesized a NIR fluorogenic probe, NI-1, that can visualize HSA in lysosomes (Fig. 8e).[67] NI-1 has a rotatable polymethine chain and a malononitrile structure for lysosome targeting. NI-1 exhibited a 95-fold fluorescence increase at 670 nm in the presence of HSA and a 10-fold fluorescence increase at 690 nm in the presence of BSA. In live-cell fluorescence imaging, NI-1 could visualize the accumulation of HSA in lysosomes of cells. Zhang *et al.* reported Nap-NO_2 as a fluorogenic probe for the detection of HSA (Fig. 8e).[68] Nap-NO_2 has a pyridinium structure, which is further conjugated with a nitrobenzyl group, as the electron acceptor. Nap-NO_2 was almost nonfluorescent in aqueous solutions, but its fluorescence intensity at 630 nm increased 14-fold in the presence of HSA. Dai *et al.* disclosed a deep-red fluorogenic probe, NITH, that can visualize HSA (Fig. 8e).[69] NITH has a benzothiazole moiety as the electron acceptor and a 4-hydroxy-1,8-naphthalimide moiety as the electron donor. It shows little fluorescence in aqueous solutions, but its fluorescence at 610 nm increased up to 56-fold in the presence of HSA. In live-cell fluorescence imaging, NITH could detect endogenous HSA produced in cells.

Finally, probes for metal ions have a metal chelator motif in their electron-donating moiety. Li *et al.* developed a fluorogenic probe, NDI-1, for the detection of mercury ions (Hg^{2+}) (Fig. 8f).[70] NDI-1 is composed of a naphthalenedimide electron acceptor, a 2-ethylhexylamine electron donor and a di-2-picolylamine (DPA) moiety as both an electron donor and Hg^{2+} recognition structure. NDI-1 forms a TICT state due to twisting between the naphthalenedimide and DPA moieties, and its fluorescence is strongly quenched. But, when the DPA moiety binds to Hg^{2+}, the TICT state formation is suppressed and fluorescence, which is derived from the ICT state with charge separation between the naphthalenedimide and hexylamine moieties, is emitted. NDI-1 shows high selectivity for Hg^{2+}. Furthermore, reversible fluorogenic probes for Hg^{2+}, NDI-5,[71] and for Cd^{2+}, NDI-15,[72] have been reported (Fig. 8f).

4.4. BODIPY

Boron dipyrromethene (BODIPY) has been utilized as a core fluorophore for many fluorogenic probes due to its excellent properties, including resistance to light and chemicals, and relatively high molar absorption coefficient and fluorescence quantum yield.[73] The BODIPY skeleton is a good electron acceptor, and it has been reported that the introduction of an electron donor moiety into its structure promotes TICT state formation, quenching the fluorescence.[74] In this section, we describe BODIPY-based fluorogenic probes utilizing the TICT mechanism.

A fluorogenic probe, BOPIM-1 (Fig. 9a),[75] in which the dimethylaminophenyl groups of the probe serve as electron donors to form the TICT state, can detect BSA.[76] The binding of BOPIM-1 to BSA caused a blue shift of 33 nm and up to 70-fold fluorescence increase. A fluorogenic probe, BV-1, which can visualize mitochondrial viscosity, was also reported (Fig. 9b).[77] In the structure of BV-1, the BODIPY moiety acts as an electron acceptor and the 2,5-dihydroxyphenyl group acts as an electron donor for TICT state formation. The fluorescence of BV-1 increased with increasing viscosity and was localized mainly in mitochondria. Ren *et al.* described a fluorogenic probe for H_2S, BH-HS, consisting of a hemicyanine structure conjugated to the BODIPY backbone as the electron acceptor moiety and a dimethylaniline electron donor (Fig. 9c).[78] The nucleophilic attack of HS^- on the electron acceptor structure of the probe cleaves the π-conjugated system, reducing the electron-accepting character and thereby inhibiting TICT state formation. Further, a red-emitting fluorogenic BODIPY-tetrazine, in which the 1,2,4,5-tetrazine moiety acts as an electron acceptor and the BODIPY moiety acts as an electron donor for TICT state formation, quenching its fluorescence, has been reported (Fig. 9d).[79] The probe showed a large fluorescence increase upon reaction with *trans*-cyclooctene and cyclopropane, due to a change in the electron-accepting ability of the 1,2,4,5-tetrazine moiety. This approach can also be applied to increase the fluorescence quantum yield of di(4-dialkylamino)-styryl BODIPYs, which show low fluorescence quantum yields. Improved distyryl BODIPYs were developed with sulfone- and quaternary ammonium-modified piperidines as auxochromes instead of conventional dialkylamino auxochromes (Fig. 9e).[80] This structural modification markedly improved the fluorescence quantum yield due to the efficient inhibition of TICT state formation.

4.5. Rhodamine

Rhodamines possess high brightness, high photostability and high hydrophilicity, and many rhodamine-based fluorogenic probes have been developed.[81] It has been known since the 1980s that *N*-alkylated rhodamines partially form a TICT excited state, in which the alkylated amino group serves as

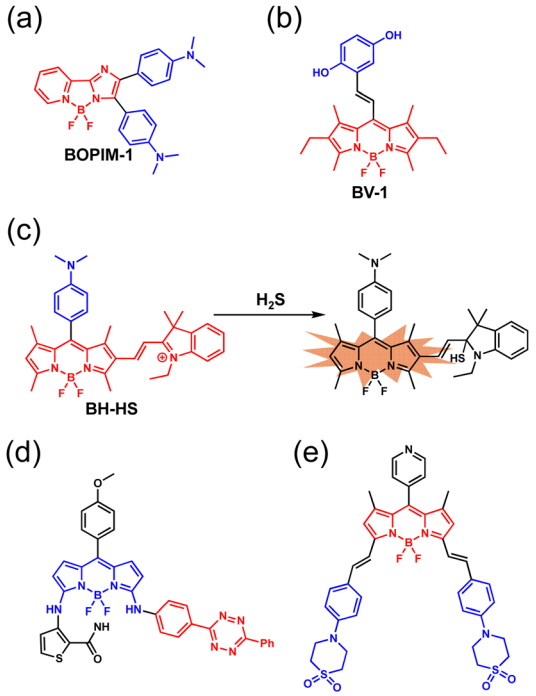

Fig. 9 TICT-based fluorogenic probes having the BODIPY scaffold. Fluorogenic probes for (a) BSA, (b) viscosity, (c) H_2S, (d) click reaction-based labelling and (e) a bright NIR distyryl BODIPY. The blue and red structures are electron-donating and -accepting moieties, respectively.

the electron donor and the xanthene ring acts as the electron acceptor.[82] However, there were few reports on the development of fluorogenic probes utilizing TICT state formation based on xanthene dye before the 2010s. One of the first TICT-based fluorogenic probes with a structure similar to that of rhodamines was Nile red (Fig. 3c), which is used for the detection of LDs, based on its strong NIR fluorescence in hydrophobic environments. It has been reported that the environmental sensitivity of Nile red is due to TICT.[21] The dye shows weak fluorescence in highly polar environments due to stabilization of the non-radiative TICT state, but shows strong fluorescence from the emissive ICT state in low-polarity environments due to the instability of its TICT state.

Recently, many rhodamine-based fluorogenic probes have employed a molecular design that promotes TICT state formation by modifying the N atom on the xanthene ring. Hirayama *et al.* reported a fluorogenic probe for Fe(ii), RhoNox-1 (Fig. 3d).[24] RhoNox-1 is based on the TICT mechanism, as shown in Fig. 3d. pH titration results indicated that the fluorescence quenching of RhoNox-1 is due to the TICT mechanism rather than the PeT mechanism. In other words, the fluorescence quenching of RhoNox-1 is derived from TICT state formation, for which the *N*-oxide group serves as the electron acceptor and the diethylamine group acts as the electron donor. Chen *et al.* described a fluorogenic probe for hydroxyl radicals (•OH), RH-EDA (Fig. 10a).[83] They found that the neuroprotective drug edaravone (3-methyl-1-phenyl-2-pyrazolin-5-one) is an excellent •OH scavenger, and they employed it as a •OH-sensitive structure. RH-EDA has a

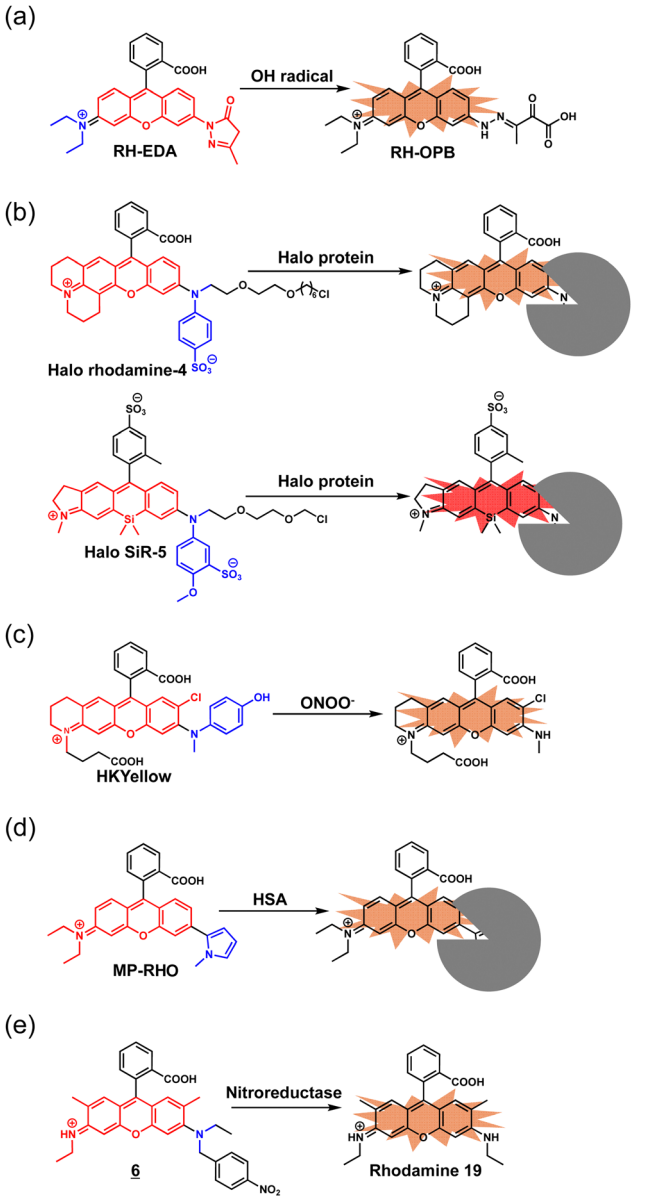

Fig. 10 TICT-based fluorogenic probes having the rhodamine scaffold. (a) Probe with modification of the N atom on the xanthene ring. (b) Ph-rhodamine-based probes for the detection of HaloTag protein. (c) Probe utilizing a phenol moiety. (d) Probe utilizing a pyrrole moiety. (e) Probe employing the sr-TICT mechanism.

3-methylpyrazolone moiety, which is a substructure of edaravone, at the 3-position of the xanthene ring. In the probe, the xanthene ring including the 3-methylpyrazolone moiety is the electron acceptor and the diethylamino group is the electron donor for TICT state formation. RH-EDA was converted to highly fluorescent RH-OPB by oxidation of the 3-methylpyrazolone moiety with •OH. The view that the fluorescence change is due to the structural change from RH-EDA to RH-OPB was supported by TD-DFT calculations.

Our group also recently reported fluorogenic probes based on Ph-rhodamines, which have a phenyl group at the N atom on the xanthene ring of the rhodamine scaffold, for the detection

of HaloTag protein, Halo rhodamine-4 and Halo SiR-5 (Fig. 10b).[84] Although many rhodamine derivatives have high fluorescence quantum yields, Ph-rhodamines show extremely low fluorescence quantum yields ($\Phi_{fl} < 0.001$). Consequently, Ph-rhodamines have been used as dark quenchers for FRET-based fluorogenic probes such as the QSY series.[85] Although the fluorescence quenching mechanism of Ph-rhodamines had long been unclear, our group recently demonstrated that the Ph-rhodamines are fluorescently quenched through a TICT process, based on the measured photophysical properties of various Ph-rhodamine derivatives together with TD-DFT calculations. The fluorescence of Halo rhodamine-4 and/or Halo SiR-5 was quenched *via* the TICT mechanism due to the free rotation of the terminal amino group on the xanthene ring before its binding to HaloTag protein. However, the probes become highly fluorescent when bound to HaloTag protein because the rotation of their terminal amino group is then inhibited by steric repulsion with the amino acid residues on the protein surface. We further demonstrated that Halo SiR-5 could visualize HaloTag-expressing neurons in 3D fluorescence imaging of the whole brain, using tissue-clearing technology.

Peng *et al.* reported a fluorogenic probe for $ONOO^-$, HKYellow, based on the Ph-rhodamine scaffold (Fig. 10c).[86] HKYellow has a phenol group on the N atom of the xanthene ring of the rhodamine scaffold and shows weak fluorescence in aqueous solutions, probably due to TICT state formation. The probe selectively reacts with $ONOO^-$ to release the phenol group and becomes highly fluorescent. They further demonstrated that HKYellow could visualize endogenous $ONOO^-$ in mouse models of acute alcohol-induced liver injury and hepatic ischemia/reperfusion injury. Miao *et al.* developed a fluorogenic probe, MP-RHO, that can detect HSA (Fig. 10d).[62] MP-RHO has an *N*-methylpyrrole structure at the end of the xanthene moiety and is colourless in neutral aqueous solutions because of intramolecular spirocycle formation. The fluorescence quantum yield of MP-RHO in water (0.1% trifluoroacetic acid) was a very low (Φ_{fl} = 0.003) because the *N*-methyl pyrrole moiety acts as an electron donor and the xanthene ring moiety serves as an electron acceptor, forming a TICT state. MP-RHO exhibited a 782-fold fluorescence increase upon addition of HSA.

Our group recently reported that TICT-based fluorogenic probes having the 2-Me rhodamine scaffold are useful for the detection of enzyme activities (Fig. 3b and 10e).[20,87] The introduction of a Me group at the 2-position of the xanthene ring strongly induced TICT state formation, and the compound showed little fluorescence. Based on the photophysical properties and TD-DFT calculations of a series of these rhodamine derivatives, we have shown that the intramolecular twisting of the dyes in the ground state due to steric repulsion between the Me group at the 2-position of the xanthene ring and two Me groups on the N atom greatly accelerates TICT state formation in the excited state. Further, when the steric repulsion was cancelled by the structural change of the probe upon reaction with the target molecule, TICT state formation was no longer promoted and the probe reverted to a strongly fluorescent state. We named this fluorescence off/on mechanism steric repulsion-induced TICT (sr-TICT).[20] On the basis of this mechanism, we have developed a fluorogenic probe for the detection of CYP3A4 activity, 2-Me PeER. The fluorescence of 2-Me PeER was strongly quenched through the sr-TICT mechanism, but the probe became highly fluorescent when the alkyl chain of the N atom on the xanthene ring was removed by CYP3A4, eliminating the steric repulsion. We found that 2-Me PeER enabled the enrichment of the mature intestinal epithelial-like cells by means of CYP3A4 activity-based fluorescence-activated cell sorting (FACS). Moreover, the combination of the sr-TICT mechanism with azaquinone methide chemistry afforded a fluorogenic probe **6** that can detect nitroreductase activity (Fig. 10e).[87] The introduction of a 4-nitrobenzyl group at the N atom of the xanthene ring of rhodamine 19 resulted in strong fluorescence quenching through the sr-TICT mechanism, and the reduction of a nitro group to an amino group by nitroreductases eliminated the azaquinone methide to afford highly fluorescent rhodamine 19.

In most TICT-based fluorogenic probes having the rhodamine scaffold, modification of an N atom on the xanthene ring promotes TICT state formation and quenches the fluorescence. So, to develop multi-functional TICT-based fluorogenic probes, asymmetric rhodamines are preferred as fluorophore cores. Further, the wavelength of the rhodamines can be extended to the far-red to NIR region by changing the O atom at the 10-position of the xanthene ring to a C, Si or P atom. We have recently reported synthetic methods for asymmetric Si-rhodamines, in which the O atom at the 10-position of the xanthene ring is replaced by an Si atom,[88] representing a further development in the evolution of TICT-based fluorogenic probes having the xanthene scaffold.

5. TICT-based design strategies for photosensitizers and chemiluminescent probes

TICT-based activatable photosensitizers for cancer therapy have been reported. Han *et al.* developed C2–NO_2 as an activatable photosensitizer for photodynamic therapy (Fig. 11a).[89] They found that the introduction of an electron-withdrawing group at the C2′ position promotes TICT state formation of the fluorophore, while the introduction of an electron-donating group favors the formation of an excited triplet state of the fluorophore through intersystem crossing (ISC) *via* PeT. C2–NO_2 with a nitro group produces reactive oxygen species at low levels because it forms a TICT state after photoirradiation, whereas C2–NH_2, formed by the nitroreductase-mediated reduction of C2–NO_2, produces reactive oxygen species *via* the formation of an excited triplet state. Administration of C2–NO_2 to tumor-model mice, followed by light irradiation at 671 nm, resulted in the inhibition of tumour growth.

The TICT mechanism has recently been reported to be applicable to control not only fluorescence, but also chemiluminescence. Zhang *et al.* reported the TICT-based photoactivatable chemiluminescent probes DCM-gal-CF and QM-B-CF (Fig. 11b and c).[90]

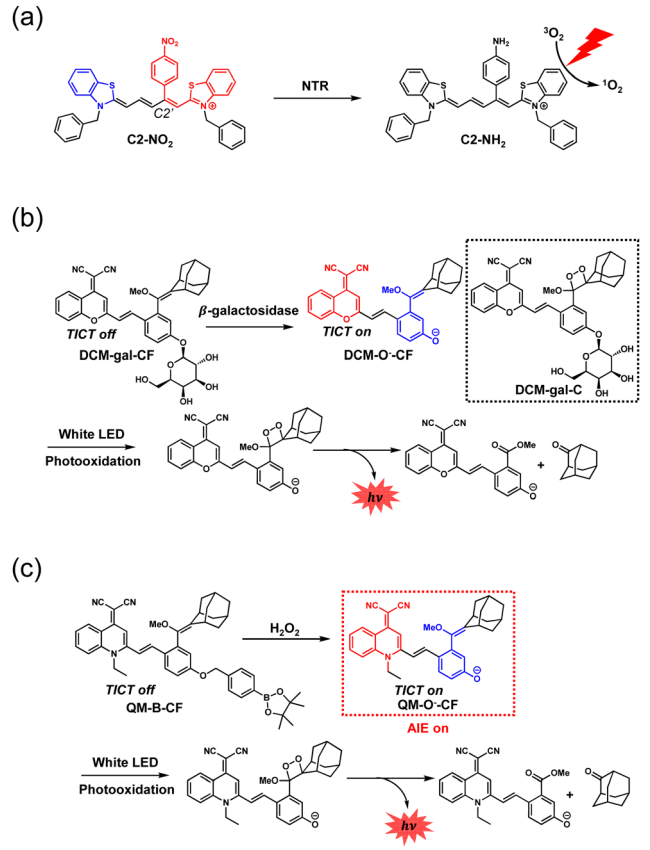

Fig. 11 TICT-based photosensitizers and chemiluminescent probes. (a) Photosensitizer; (b) chemiluminescent probes for β-galactosidase and light; (c) chemiluminescent probes for H_2O_2 and light. The blue and red structures are the electron-donating and -accepting moieties, respectively.

Although several dioxetane-based chemiluminescent probes had been already reported,[91] the unstable phenolate-dioxetane generated by the reaction of the chemiluminescent probes with analytes shows spontaneous glow-type emission, resulting in a weak signal intensity. Zhang *et al.* found that the chemiluminescence intensity can be enhanced by molecular design based on a dual-locking strategy that combines the analyte reaction with photo-oxidation modulated by the TICT process. TD-DFT calculations showed that the TICT state of DCM-gal-CF or QM-B-CF is unstable, while that of DCM-O^--CF or QM-O^--CF, which is formed after reaction with the analyte (β-galactosidase or H_2O_2), is stable. DCM-O^--CF or QM-O^--CF forms a 1,2-dioxetane skeleton *in situ via* TICT-based radical addition with O_2 under white LED illumination. Consequently, a high concentration of unstable phenolate-dioxetane can be produced. DCM-gal-CF exhibited a 9.5-fold luminescence increase compared to single-locked DCM-gal-C. They took advantage of the fact that QM-O^--CF exhibits aggregation-induced emission (AIE) in water to track pre-chemiluminophore aggregation (Fig. 11c).

Conclusions

This review focuses on the molecular design of fluorogenic probes utilizing the TICT mechanism. TICT is a versatile fluorescence control method that can be applied to various fluorophores, including not only typical dye scaffolds such as cyanine, coumarin, 1,8-naphthimide, BODIPY and rhodamine, but also other dye scaffolds.[92–96] The mechanism involves intramolecular charge separation arising from a structural change to the twisting conformation of electron donor and electron acceptor moieties, which is highly sensitive to the environment of the dye (polarity, viscosity, *etc.*). Initially, probes were mainly developed to recognize macrobiomolecules such as DNA and HSA/BSA and respond with a large fluorescence increase. More recently, structural modifications of the electron donor and acceptor moieties of fluorogenic probes have been extensively employed to control the stability of the TICT excited state. Further, it is becoming possible to accurately predict the stability of the TICT excited state by means of TD-DFT quantum chemical calculations because of the improving understanding of the TICT-related fluorescence quenching mechanism. TD-DFT calculations of the S_1 potential energy surface can predict the rotation barrier energy and the stabilization energy of the TICT excited state compared to the energy before rotation. Since structural modification can control these energies, rational design of TICT-based fluorogenic probes can be performed by calculating these energies of TICT-based fluorophores.[93] For example, a TICT-based fluorogenic probe that can detect CYP3A4 activity, reported by our group, would have been difficult to develop empirically. This achievement highlights the usefulness of the TICT mechanism as a fluorescence control principle.[20] Moreover, it has also recently been shown that the TICT mechanism can be applied to the off/on control of not only fluorescence, but also photosensitizing and chemiluminescence ability. Application to detect other functional molecules can be expected. Thus, we believe the TICT mechanism represents a practical method for controlling the photophysical properties of probes, and will greatly facilitate the development of a range of chemical tools for medicine and life science.

Conflicts of interest

There are no conflicts to declare.

Data availability

No primary research results, software or code have been included and no new data were generated or analysed as part of this review.

Acknowledgements

This work was supported in part by JSPS KAKENHI Grant Numbers JP23K27304, JP23K20040, JP23K17389, JP21H05262 and 24K01446 to K. H., a grant from the Japan Agency for Medical Research and Development (AMED) (JP24ak0101182 s0104 and JP24gm1510012s0202) to K.H., JST CREST to K. H. and Program for the Advancement of Next Generation Research

Projects (Keio University), Academic Development Fund (Keio University Academic Development Funds) and Fukuzawa Fund (Keio Gijuku Fukuzawa Memorial Fund for the Advancement of Education and Research) to K.H., and World Premier International Research Center Initiative (WPI), MEXT, Japan.

Notes and references

1 T. Ueno and T. Nagano, *Nat. Methods*, 2011, **8**, 642–645.
2 G. Grynkiewicz, M. Poenie and R. Y. Tsien, *J. Biol. Chem.*, 1985, **260**, 3440–3450.
3 B. N. G. Giepmans, S. R. Adams, M. H. Ellisman and R. Y. Tsien, *Science*, 2006, **312**, 217–224.
4 Y. Urano, M. Kamiya, K. Kanda, T. Ueno, K. Hirose and T. Nagano, *J. Am. Chem. Soc.*, 2005, **127**, 4888–4894.
5 Z. R. Grabowski, K. Rotkiewicz and W. Rettig, *Chem. Rev.*, 2003, **103**, 3899–4031.
6 E. Lippert, W. Lüder, F. Moll, W. Nägele, H. Boos, H. Prigge and I. Seibold-Blankenstein, *Angew. Chem.*, 1961, **73**, 695–706.
7 G. Jones II, W. R. Jackson, C. Y. Choi and W. R. Bergmark, *J. Phys. Chem.*, 1985, **89**, 294–300.
8 T. Karstens and K. Kobs, *J. Phys. Chem.*, 1980, **84**, 1871–1872.
9 M. Cooper, A. Ebner, M. Briggs, M. Burrows, N. Gardner, R. Richardson and R. West, *J. Fluoresc.*, 2004, **14**, 145–150.
10 J. B. Grimm, B. P. English, J. Chen, J. P. Slaughter, Z. Zhang, A. Revyakin, R. Patel, J. J. Macklin, D. Normanno, R. H. Singer, T. Lionnet and L. D. Lavis, *Nat. Methods*, 2015, **12**, 244–250.
11 Z. Ye, W. Yang, C. Wang, Y. Zheng, W. Chi, X. Liu, Z. Huang, X. Li and Y. Xiao, *J. Am. Chem. Soc.*, 2019, **141**, 14491–14495.
12 X. Lv, C. Gao, T. Han, H. Shi and W. Guo, *Chem. Commun.*, 2020, **56**, 715–718.
13 C. A. Hoelzel, H. Hu, C. H. Wolstenholme, B. A. Karim, K. T. Munson, K. H. Jung, H. Zhang, Y. Liu, H. P. Yennawar, J. B. Asbury, X. Li and X. Zhang, *Angew. Chem., Int. Ed.*, 2020, **59**, 4785–4792.
14 C. Wang, Q. Qiao, W. Chi, J. Chen, W. Liu, D. Tan, S. McKechnie, D. Lyu, X.-F. Jiang, W. Zhou, N. Xu, Q. Zhang, Z. Xu and X. Liu, *Angew. Chem., Int. Ed.*, 2020, **59**, 10160–10172.
15 D. R. Rogers, *Am. J. Clin. Pathol.*, 1965, **44**, 59–61.
16 A. A. Maskevich, V. I. Stsiapura, V. A. Kuzmitsky, I. M. Kuznetsova, O. I. Povarova, V. N. Uversky and K. K. Turoverov, *J. Proteome Res.*, 2007, **6**, 1392–1401.
17 V. I. Stsiapura, A. A. Maskevich, V. A. Kuzmitsky, V. N. Uversky, I. M. Kuznetsova and K. K. Turoverov, *J. Phys. Chem. B*, 2008, **112**, 15893–15902.
18 V. I. Stsiapura, A. A. Maskevich, V. A. Kuzmitsky, K. K. Turoverov and I. M. Kuznetsova, *J. Phys. Chem. A*, 2007, **111**, 4829–4835.
19 A. I. Dragan, R. Pavlovic, J. B. McGivney, J. R. Casas-Finet, E. S. Bishop, R. J. Strouse, M. A. Schenerman and C. D. Geddes, *J. Fluoresc.*, 2012, **22**, 1189–1199.
20 K. Hanaoka, T. Ikeno, S. Iwaki, S. Deguchi, K. Takayama, H. Mizuguchi, F. Tao, N. Kojima, H. Ohno, E. Sasaki, T. Komatsu, T. Ueno, K. Maeda, H. Kusuhara and Y. Urano, *Sci. Adv.*, 2024, **10**, eadi8847.
21 C. M. Golini, B. W. Williams and J. B. Foresman, *J. Fluoresc.*, 1998, **8**, 395–404.
22 A. S. Klymchenko, *Acc. Chem. Res.*, 2023, **56**, 1–12.
23 E. Prifti, L. Reymond, M. Umebayashi, R. Hovius, H. Riezman and K. Johnsson, *ACS Chem. Biol.*, 2014, **9**, 606–612.
24 T. Hirayama, K. Okuda and H. Nagasawa, *Chem. Sci.*, 2013, **4**, 1250–1256.
25 A. Mishra, R. K. Behera, P. K. Behera, B. K. Mishra and G. B. Behera, *Chem. Rev.*, 2000, **100**, 1973–2011.
26 L. Zhang, G. Li, H. Zheng and W. Lin, *New J. Chem.*, 2024, **48**, 4565–4569.
27 T. Zhang, F. Huo and C. Yin, *Sens. Actuators, B*, 2024, **404**, 135236.
28 J. Cao, C. Hu, W. Sun, Q. Xu, J. Fan, F. Song, S. Sun and X. Peng, *RSC Adv.*, 2014, **4**, 13385–13394.
29 S. Jarollahi, P. Ring and B. M. White-Mathieu, *Trends Chem.*, 2025, **7**, 11–25.
30 Y. Wang, R. Zhou, W. Liu, C. Liu and P. Wu, *Chin. Chem. Lett.*, 2020, **31**, 2950–2954.
31 R. S. Tuma, M. P. Beaudet, X. Jin, L. J. Jones, C. Y. Cheung, S. Yue and V. L. Singer, *Anal. Biochem.*, 1999, **268**, 278–288.
32 R. E. Johnson, A. Pounder, J. van der Zalm, A. Chen, I. J. Bell, T. J. Van Raay, S. D. Wetmore and R. A. Manderville, *Anal. Chem.*, 2024, **96**, 16252–16259.
33 S. I. Reja, I. A. Khan, V. Bhalla and M. Kumar, *Chem. Commun.*, 2016, **52**, 1182–1185.
34 S. Samanta, S. Halder and G. Das, *Anal. Chem.*, 2018, **90**, 7561–7568.
35 S. Samanta, M. Huang, F. Lin, P. Das, B. Chen, W. Yan, J.-J. Chen, K. Ji, L. Liu, J. Qu and Z. Yang, *Anal. Chem.*, 2020, **92**, 1541–1548.
36 R. Tian, Q. Zeng, S. Zhu, J. Lau, S. Chandra, R. Ertsey, K. S. Hettie, T. Teraphongphom, Z. Hu, G. Niu, D. O. Kiesewetter, H. Sun, X. Zhang, A. L. Antaris, B. R. Brooks and X. Chen, *Sci. Adv.*, 2019, **5**, eaaw0672.
37 R. Tian, X. Feng, L. Wei, D. Dai, Y. Ma, H. Pan, S. Ge, L. Bai, C. Ke, Y. Liu, L. Lang, S. Zhu, H. Sun, Y. Yu and X. Chen, *Nat. Commun.*, 2022, **13**, 2853.
38 L. Bai, Z. Hu, T. Han, Y. Wang, J. Xu, G. Jiang, X. Feng, B. Sun, X. Liu, R. Tian, H. Sun, S. Zhang, X. Chen and S. Zhu, *Theranostics*, 2022, **12**, 4536–4547.
39 W. Hu, Y. He, H. Ren, L. Chai, H. Li, J. Chen, C. Li, Y. Wang and T. D. James, *Chem. Sci.*, 2024, **15**, 6028–6035.
40 L. Zhu, J. Xu, Z. Sun, B. Fu, C. Qin, L. Zeng and X. Hu, *Chem. Commun.*, 2015, **51**, 1154–1156.
41 Y. Yuan, S. Xiong, L. Lv, W. Hu, X. Xiong, C. Li and H. Deng, *Chem. Eng. J.*, 2023, **471**, 144341.
42 D. Cao, Z. Liu, P. Verwilst, S. Koo, P. Jangjili, J. S. Kim and W. Lin, *Chem. Rev.*, 2019, **119**, 10403–10519.
43 G. Jones II, W. R. Jackson and A. M. Halpern, *Chem. Phys. Lett.*, 1980, **72**, 391–395.
44 G. Jones II, W. R. Jackson, S. Kanoktanaporn and A. M. Halpern, *Opt. Commun.*, 1980, **33**, 315–320.
45 A. Nag and K. Bhattacharyya, *Chem. Phys. Lett.*, 1990, **169**, 12–16.
46 L. Chen, Y. Feng, Y. Dang, C. Zhong and D. Chen, *Anal. Bioanal. Chem.*, 2020, **412**, 7819–7826.
47 Y. Liang, Y. Zhao, C. Lai, X. Zou and W. Lin, *J. Mater. Chem. B*, 2021, **9**, 8067–8073.
48 E. Zhang, S. Wang, G. Zhang, A. Li, W. Kong, Y. Zhao, M. Xiang, R. Kong, P. Ju and F. Qu, *Talanta*, 2025, **281**, 126860.
49 X.-Y. Sun, X. Zhang, K. Gao, W.-J. Zhao, Y.-T. Tian, T. Liu and Z.-L. Lu, *Anal. Methods*, 2024, **16**, 3839–3846.
50 Y.-Y. Li, J.-L. Hu, J.-R. Wu, Y.-R. Wang, A.-H. Zhang, Y.-W. Tan, Y.-J. Shang, T. Liang, M. Li, Y.-L. Meng and Y.-F. Kang, *Biosens. Bioelectron.*, 2024, **254**, 116233.
51 Y. Wang, Y. Zhong, Q. Wang, X.-F. Yang, Z. Li and H. Li, *Anal. Chem.*, 2016, **88**, 10237–10244.
52 T. Debnath, P. Maity, H. Lobo, B. Singh, G. S. Shankarling and H. N. Ghosh, *Chem. – Eur. J.*, 2014, **20**, 3510–3519.
53 T. Debnath, J. Dana, P. Maity, H. Lobo, G. S. Shankarling and H. N. Ghosh, *Chem. – Eur. J.*, 2015, **21**, 5704–5708.
54 Q. Sun, H. Tian, H. Qu, D. Sun, Z. Chen, L. Duan, W. Zhang and J. Qian, *Analyst*, 2015, **140**, 4648–4653.
55 G. Anwar, D. Chen, Q. Chen, C. Xia and J. Yan, *Spectrochim. Acta A Mol. Biomol. Spectrosc.*, 2024, **307**, 123637.
56 I. A. Karpenko, Y. Niko, V. P. Yakubovskyi, A. O. Gerasov, D. Bonnet, Y. P. Kovtun and A. S. Klymchenko, *J. Mater. Chem. C*, 2016, **4**, 3002–3009.
57 W. Nie and L. Hu, *ChemistrySelect*, 2024, **9**, e202303779.
58 Y.-F. Wei, X.-Q. Zhang, R. Sun, Y.-J. Xu and J.-F. Ge, *Dyes Pigm.*, 2021, **194**, 109559.
59 T. Liu, X. Liu, D. R. Spring, X. Qian, J. Cui and Z. Xu, *Sci. Rep.*, 2014, **4**, 5418.
60 D. Wei, Y. Dai, J. Cao and N. Fu, *Anal. Chim. Acta*, 2024, **1299**, 342422.
61 F. Meng, J. Niu, H. Zhang, R. Yang, Q. Lu, Y. Yu, Z. Liu, G. Niu and X. Yu, *Sens. Actuators, B*, 2021, **329**, 129148.
62 R. Miao, J. Li, C. Wang, X. Jiang, Y. Gao, X. Liu, D. Wang, X. Li, X. Liu and Y. Fang, *Adv. Sci.*, 2022, **9**, 2104609.
63 X.-C. Feng, G. Zhang, R. Sun, Y.-J. Xu and J.-F. Ge, *Sens. Actuators, B*, 2023, **394**, 134469.
64 L. Michel, P. Durand and A. Chevalier, *ChemBioChem*, 2024, **25**, e202400270.

65 W. Jiang, Q. Qiao, J. Chen, P. Bao, Y. Tao, Y. Zhang and Z. Xu, *Adv. Sci.*, 2024, **11**, 2309743.
66 G.-S. Wu, N. Thirumalaivasan, T.-C. Lin and S.-P. Wu, *J. Pharm. Biomed. Anal.*, 2020, **190**, 113545.
67 Y. Ke, J. Cao, J. Gong and N. Fu, *Sens. Actuators, B*, 2022, **352**, 131015.
68 M. Zhang, J. Cao, C. Huang, M. Liu, Y. Li, C. Wang and Y. Tu, *Dyes Pigm.*, 2023, **208**, 110867.
69 Y. Dai, J. Gong, J. Cao, W. Chen and N. Fu, *Dyes Pigm.*, 2024, **222**, 111893.
70 Q. Li, M. Peng, H. Li, C. Zhong, L. Zhang, X. Cheng, X. Peng, Q. Wang, J. Qin and Z. Li, *Org. Lett.*, 2012, **14**, 2094–2097.
71 L. Zong, Y. Xie, Q. Li and Z. Li, *Sens. Actuators, B*, 2017, **238**, 735–743.
72 L. Zong, M. Zhang, Y. Song, Y. Xie, J. Feng, Q. Li and Z. Li, *Sens. Actuators, B*, 2018, **257**, 882–888.
73 N. Boens, V. Leen and W. Dehaen, *Chem. Soc. Rev.*, 2012, **41**, 1130–1172.
74 R. Hu, E. Lager, A. Aguilar-Aguilar, J. Liu, J. W. Y. Lam, H. H. Y. Sung, I. D. Williams, Y. Zhong, K. S. Wong, E. Peña-Cabrera and B. Z. Tang, *J. Phys. Chem. C*, 2009, **113**, 15845–15853.
75 C. Liu, W. Yang, J. Du, P. Shen and C. Yang, *Photochem. Photobiol.*, 2017, **93**, 1414–1422.
76 P. Shen, S. Xiao, X. Zhan, W. Zhang, K. Chang and C. Yang, *J. Phys. Org. Chem.*, 2013, **26**, 858–862.
77 M. Sun, T. Wang, X. Yang, H. Yu, S. Wang and D. Huang, *Talanta*, 2021, **225**, 121996.
78 M. Ren, B. Deng, X. Kong, K. Zhou, K. Liu, G. Xu and W. Lin, *Chem. Commun.*, 2016, **52**, 6415–6418.
79 L. Chen, F. Li, Y. Li, J. Yang, Y. Li and B. He, *Chem. Commun.*, 2022, **58**, 298–301.
80 X. Lv, T. Han, Y. Wu, B. Zhang and W. Guo, *Chem. Commun.*, 2021, **57**, 9744–9747.
81 L. Wang, W. Du, Z. Hu, K. Uvdal, L. Li and W. Huang, *Angew. Chem., Int. Ed.*, 2019, **58**, 14026–14043.
82 M. Vogel, W. Rettig, R. Sens and K. H. Drexhage, *Chem. Phys. Lett.*, 1988, **147**, 452–460.
83 L. Chen, X. Wu, H. Yu, L. Wu, Q. Wang, J. Zhang, X. Liu, Z. Li and X.-F. Yang, *Anal. Chem.*, 2021, **93**, 14343–14350.
84 K. Hanaoka, S. Iwaki, K. Yagi, T. Myochin, T. Ikeno, H. Ohno, E. Sasaki, T. Komatsu, T. Ueno, M. Uchigashima, T. Mikuni, K. Tainaka, S. Tahara, S. Takeuchi, T. Tahara, M. Uchiyama, T. Nagano and Y. Urano, *J. Am. Chem. Soc.*, 2022, **144**, 19778–19790.
85 T. Myochin, K. Hanaoka, S. Iwaki, T. Ueno, T. Komatsu, T. Terai, T. Nagano and Y. Urano, *J. Am. Chem. Soc.*, 2015, **137**, 4759–4765.
86 T. Peng, X. Chen, L. Gao, T. Zhang, W. Wang, J. Shen and D. Yang, *Chem. Sci.*, 2016, **7**, 5407–5413.
87 M. Sugimoto, E. Sasaki, H. Ohno, T. Ikeno, S. Yamada and K. Hanaoka, *Chem. Pharm. Bull.*, 2024, **72**, 810–816.
88 K. Hanaoka, Y. Kagami, W. Piao, T. Myochin, K. Numasawa, Y. Kuriki, T. Ikeno, T. Ueno, T. Komatsu, T. Terai, T. Nagano and Y. Urano, *Chem. Commun.*, 2018, **54**, 6939–6942.
89 F. Han, S. A. Abbas Abedi, S. He, H. Zhang, S. Long, X. Zhou, S. Chanmungkalakul, H. Ma, W. Sun, X. Liu, J. Du, J. Fan and X. Peng, *Adv. Sci.*, 2024, **11**, 2305761.
90 Y. Zhang, C. Yan, C. Wang, Z. Guo, X. Liu and W.-H. Zhu, *Angew. Chem., Int. Ed.*, 2020, **59**, 9059–9066.
91 J. S. Sidhu, G. Kaur, A. R. Chavan, M. K. Chahal and R. Taliyan, *Analyst*, 2024, **149**, 5739–5761.
92 S. Shao, T. Yang and Y. Han, *Sens. Actuators, B*, 2023, **392**, 134041.
93 C. Wang, W. Chi, Q. Qiao, D. Tan, Z. Xu and X. Liu, *Chem. Soc. Rev.*, 2021, **50**, 12656–12678.
94 S. Sasaki, G. P. C. Drummen and G. Konishi, *J. Mater. Chem.*, 2016, **4**, 2731–2743.
95 L. Meng, S. Jiang, M. Song, F. Yan, W. Zhang, B. Xu and W. Tian, *ACS Appl. Mater. Interfaces*, 2020, **12**, 26842–26851.
96 X. Wang, L. Wang, T. Jin, K. Sun and J. Yang, *Sens. Actuators, B*, 2023, **375**, 132935.

